Proceedings of the 21st ICSMGE, Vienna, Austria, 14 – 19 June 2026. Pistrol, Adam & Schweiger (eds.)
Published by: ÖGG, Austrian Society for Geomechanics, Salzburg, Austria, ISBN 978-3-9503898-4-5
https://doi.org/10.53243/ICSMGE2026-899

Damage measures of low-rise building foundations on layered sands due to seismic impacts

Der-Wen Chang
Tamkang University, New Taipei City, Taiwan, dwchang@mail.tku.edu.tw

Askar Zhussupbekov, Diyar Mukhanov
L.N. Gumilyov Eurasian National University, Astana, Kazakhstan

Shih-Hao Cheng
National Taiwan University of Science and Technology, Taipei, Taiwan

Louis Ge, Yu-Wei Hwang
National Taiwan University, Taipei, Taiwan

Ricky K.-N. Wong
Sanshin Corporation, Taipei, Taiwan

ABSTRACT: The seismic behaviors of low-rise building foundations on liquefiable sites were studied using Midas GTS-NX analysis with the UBCSand model. Both raft and piled raft foundation models were examined on multi-layered sands. While the 2D analyses were the main tools, a few 3D analyses were carried out on the piled raft foundation. The displacements, tilts, and angular variables of the foundation were analyzed for the likely damages of the foundations based on the local design specifications. It was found that a thicker mat is useful to reduce the tilt and angular variable of the foundations. Both the raft and the piled raft foundations had considerable settlements at the intensity levels of V^+ and VI^-. Piles with longer length can yield accessible foundation settlements. For higher groundwater table cases, it was found that the underneath raft was uplifted during the seismic excitation. With the limited cases on piled raft foundations, the 2D analysis was found to provide more conservative results in comparison with the 3D analysis. If a near-fault site is encountered, the coupled ground motions will have more significant influence on settlements rather than horizontal displacements.

KEYWORDS: Low-rise building foundation, raft, piled raft, damage measures, multi-layered sand, soil liquefaction.

1 INTRODUCTION

A few recent earthquakes occurred in Taiwan were found causing damages to low-rise buildings in the suburban areas. Soil liquefaction was found at the sites. The low-rise buildings of three- to five-story reinforced concrete structures are mainly built for residential houses. The foundation of these structures is mostly made by single footings or the combined footings. Lu *et al.* (2017) examined several such building structure damages with a preliminary analysis to conclude that these foundations are vulnerable to the soil liquefaction during the earthquake. Therefore, alternate foundations such as the mat foundation and/or the piled raft foundation for such building structures are of interest. In this study, the aimed foundations were investigated with a series of finite element models based on multilayered sands. Seismic intensity levels at IV, V^-, V^+ and VI^- were considered for the time-dependent dynamic analyses, both the free-field and foundation responses were obtained for comparisons. The free-field solutions were also compared with the empirical liquefaction potential analysis for practical concerns. Damage measures of the foundation settlements, tilts and angular variables were then analyzed and compared to the design specifications (MOI, 2023). Design applications are thus suggested.

2 NUMERICAL MODELLING

2.1 *Muti-layered sand profile*

A multi-layered sand profile was considered with thickness of 50m. The groundwater table was assumed to be GL-2m. The Gibson soil profile where $G(z)=G(1+z)^{0.33}$ (G=shear modulus of the soil, z=depth of the soil) was used to model the layered stiffness. The shear wave velocity of the soil (V_s) at the ground surface was set to 130m/s. With the presumed Poisson's ratio (ν), the modulus G and E of the soil can be obtained. The soil profile was then divided into five sublayers. Empirical formulas between V_s and SPT-N values, and SPT-N vs ϕ' were used to compute the values of N and ϕ'. The friction angle of sand (ϕ') was reduced to obtain the friction angle (δ) between the sand and concrete. After calibrating the SPT-N values with the depth and the energy ratio (ER), the values of $N_{1,60}$ were obtained. Relative density (D_r) was then obtained from $N_{1,60}$ (Idriss and Boulanger, 2008). For soil liquefactions occurred during seismic excitations, the UBCSand model (Byrne *et al.*, 2003 and 2004) was adopted. Table 1 summarizes the geological soil profile and major material parameters used in this study.

Table 1. Soil profile model and material parameters.

Layer	Depth (m)	γ (kN/m^3)	V_s (m/s)	G (MPa)	ν	E (MPa)	SPT-N	$N_{1,60}$	ϕ'	D_r (%)
1	0-2	18	144	38	0.3	99	5	7	28°	39
2	2-10	20	165	55	0.4	155	8	10	30°	47
3	10-20	20	186	71	0.4	199	12	12	32°	51
4	20-30	20	201	82	0.4	230	15	12	33°	51
5	30-50	20	215	94	0.4	264	19	12	35°	51

NOTE: $V_s = 80(N)^{0.333}$; $\phi' = 3.5(N)^{0.5}+20$; $N_{1,60} = C_N \times N \times (ER/60)$ where $C_N = (Pa/\sigma'_0)0.5$, $0.5 \le CN \le 1.6$, $ER(\%) = 30(z/11)+50$ for $z \le 11m$ and $ER(\%) = 80$ for $z \ge 11m$; $Dr = (N_{1,60}/C_d)^{0.5}$, C_d: calibration factor = 46 (Idriss and Boulanger, 2008)

Note that the empirical relationships used for the material parameters are also presented in Table 1. Corresponding material parameters used in UBCSand model are summarized in Table 2. The model parameters were initially established through a comparative study using data from Byrne *et al*. (2003 and 2004) on the centrifuge tests and FLAC analyses. Midas-GTS NX analysis (Midas, 2020) was adopted for the

comparisons. Additionally, the data of the dynamic triaxial test and the cyclic simple shear test (Ko, 2023) were studied using a single element. These model calibration studies were carried out to ensure the UBCSand model parameters selected in this study are fair enough with respect to the fundamental material parameters such as $(N1)_{60}$ and relative density of the liquefiable sand. The details of the comparison study can be found in Lien (2024) and Hsu (2025[b]).

Table 2. UBCSand model parameters used in this study.

Layer	Depth (m)	K_G^e	ne	ϕ_p	ϕ_{cv}	K_G^p	np	R_f
1	0-2	895	0.5	29°	28°	231	0.4	0.82
2	2-10	627	0.5	31°	30°	288	0.4	0.78
3	10-20	547	0.5	33°	32°	336	0.4	0.76
4	20-30	498	0.5	34°	33°	315	0.4	0.76
5	30-50	456	0.5	36°	35°	297	0.4	0.76

2.2 *Finite element models*

For the raft and the piled raft foundations, the standard and varying dimensions of the foundations and the parameters can be found in Hsu (2025[b]). The Midas-GTS NX Finite Element (FE) analysis (Midas, 2020) was chosen to analyze the seismic response. Figure 1 illustrates the plane-view of the 2D FE mesh of the free-field soil profile and the profile where the raft foundation and the piled raft foundation located. They were examined carefully to ensure that the mesh can provide stable and rational solutions. Note that the Q4 and T3 elements were used in the mesh. Aspect ratio requirement of the elements was followed to ensure that the solutions are rational.

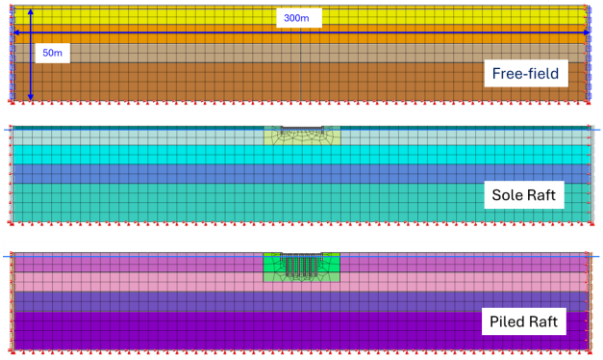

Figure 1. The dimensions and mesh of FE model.

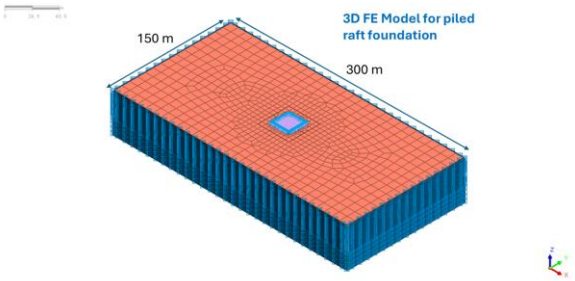

Figure 2. The 3D FE mesh for piled raft foundation analysis.

For foundation model, a 1.5m-thick slab was presumed. Uniformly static structural load was applied on top of the foundation. Note that the infinity type of boundary (free field) conditions was applied at the lateral sides of FE mesh to simulate the waves transmitting through the boundaries. At the bottom side, the hinges were implemented because no relative displacement was presumed between the soils and underlain bedrock. The Coulomb type of interface element was used to simulate the frictions between soil and concrete. The tangential stiffness K_t of the interface element was kept as 1/10 of the normal stiffness K_n of the element, whereas the value of K_n was determined as ten times of the Young's modulus of the soil. The ultimate friction of the element was governed by the reduced friction angle of the soil. The ratio was kept at 0.67. For validations, the 3D analysis was conducted especially for piled raft foundation. Figure 2 illustrates the 3D FE model in use. It was examined to ensure that the solutions were stable and rational. The thickness of the 3D mesh in the transverse direction (or the off-plane direction) was extended to 150m. Only square mat was considered in the study. Figure 3 reveals the locations for observations in this study. Table 3 summarizes the foundation models and their dimensions.

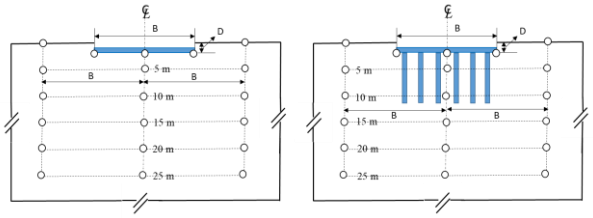

Figure 3. Observation locations of the numerical model.

Table 3. Foundation models and their dimensions.

Sole raft foundation	Standard dimensions: raft width (B)=20m, raft thickness (t_r)=1.5m, embedded depth (D)=2m, side wall depth (H)=2×h, side wall thickness (t_w)= 0.7m, load intensity of superstructure (q)=30 kPa. Independent varying dimensions: B=30m, D=5m, and q=60 kPa
Piled raft foundation	Standard dimensions: same dimensions as the standard raft, pile diameter (d)=1m, pile length (l)=10m, pile-to-pile spacing distance (S)=3m. Independent varying dimensions: l=15m, and S=5m

Table 4. Validations of the seismic records with the numerical profile.

Vibrations	Profile *fn* (Hz)	Predominant frequency, Hz in 1999 Chi-Chi Earthquake				
		TAP003	TAP012	TAP014	TAP017	TAP026
Horizontal	0.95	0.89	1	0.98	0.94	1.16
Vertical	6.28	5	8.33	5	7.14	4.5
Vibrations	Profile *fn* (Hz)	Predominant frequency, Hz in 2002 Hualien Earthquake				
		TAP006	TAP007	TAP012	TAP019	TAP025
Horizontal	0.95	0.83	0.83	0.86	0.94	0.8
Vertical	6.28	5	5.55	8.33	4.5	4.2

3 BEDROCK MOTIONS

The time-dependent dynamic responses of the models were obtained. For simplicity, the scaling method (Kramer and Stewart, 2024) was adopted to convert the record into bedrock motions based on the target PGA (PGA_T). Local intensity levels IV, V^-, V^+ and VI^- were considered, the corresponding PGA_T at 0.07g, 0.11g, 0.195g and 0.26g were assumed. Seismic records at the station TAP012 in Taipei city during the 1999 Chi-Chi earthquake (M=7.3) and the 2002 Hualien earthquake (M=6.8) were considered with the concern that the natural characteristics of the model and the motions must be compatible. The accelerogram recorded at the EW and vertical directions and their corresponding response spectrums from Chi-Chi quake can be found in Figure 4.

Table 4 summarizes the predominated frequencies of several acceleration records from Chi-Chi and Hualien earthquakes with the natural frequencies of the numerical profile for horizontal and vertical vibrations. The acceleration records in use are proved feasible in this study. For the coupled

motion influence study, the near-fault concerns, the PGA in the vertical direction, PGA_V was kept as 2/3 of PGA_H (where PGA_H is the PGA in the horizontal direction) as it was suggested in the local seismic design code.

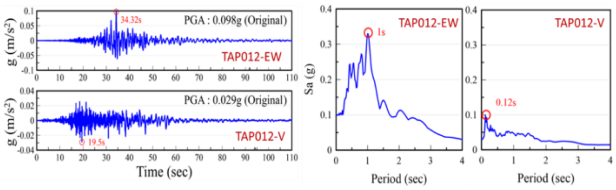

Figure 4. Seismic records of TAP012 in Chi-Chi quake.

4 LIQUEFACTION POTENTIAL ASSESSMENTS

Liquefaction potential analysis of the free-field model was first carried out using the HBF, NCREE, AIJ and JRA methods (MOI, 2023). The magnitude of the earthquake (M) was considered in the range of 7.5-6.0 (namely M1-M4 with the 0.5 order difference at their magnitudes), whereas the peak ground acceleration (PGA) was considered in the range of 0.26g~0.07g (namely A1-A4 for PGA=0.26g, 0.195g, 0.11g, and 0.07g). Combining them rationally, there were several cases found by Hsu (2025[a]) where soil liquefaction can occur easily when PGA>0.11g with different magnitudes.

Figure 5 reveals the factor of safety against soil liquefaction versus the depth of the soil for the case of M1A1 and M1A2 where the fine content effects were included. It was found that these methods can provide comparable predictions for soil liquefaction if the fine grains of the soil are rarely seen. The variations of the factors of safety from these methods were found alike for soils at GL-0m~GL-30m. The fine content can significantly affect the predictions of NCEER and AIJ methods.

The settlements of the model computed through the semi-empirical methods (Ishihara and Yoshimine, 1992 and Tokimatsu and Seed, 1987) are presented in Figure 6 with the assessments using HBF and AIJ methods assuming that the earthquake magnitude is 6.5 and 7.0 for PGA=0.195g and 0.26g. The predictions using AIJ method were found more conservative especially in adopting the Ishihara and Yoshimine method.

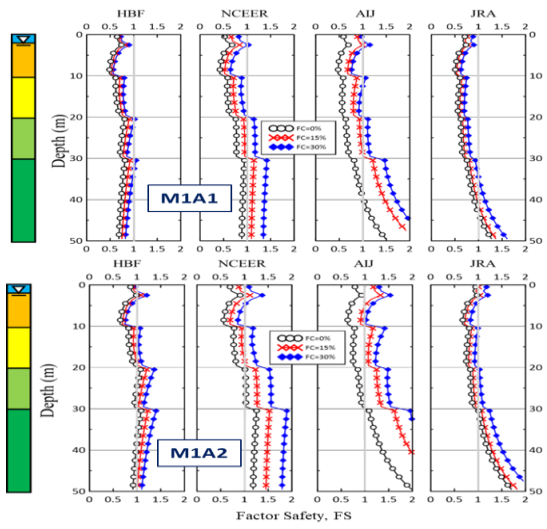

Figure 5. Liquefaction assessments of the numerical model.

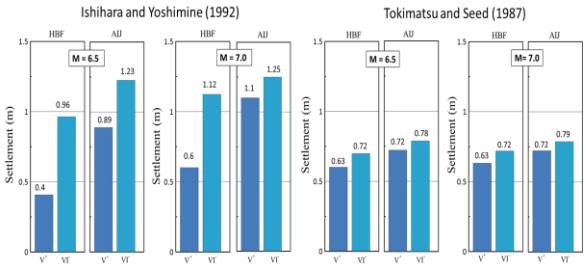

Figure 6. Seismic settlement from semi-empirical prediction methods.

5 SITE AND FOUNDATION RESPONSES

5.1 *Free field*

Figure 7 depicts the 2D analysis results showing the time histories of shear stress, shear strains, and excess pore-pressure ratios found at the free-field model (where PGA_T=0.195g with Chi-Chi record). The shear stresses were reduced when soil liquefaction occurred. The shear strains greater than 1% can cause the soil to liquefy. The top twenty meters of the soil profile was found vulnerable for liquefaction. The permanent displacement field indicates that the ground has an unbalanced movement to its left after the earthquake. Detailed discussions can be found in Hsu (2025[b]).

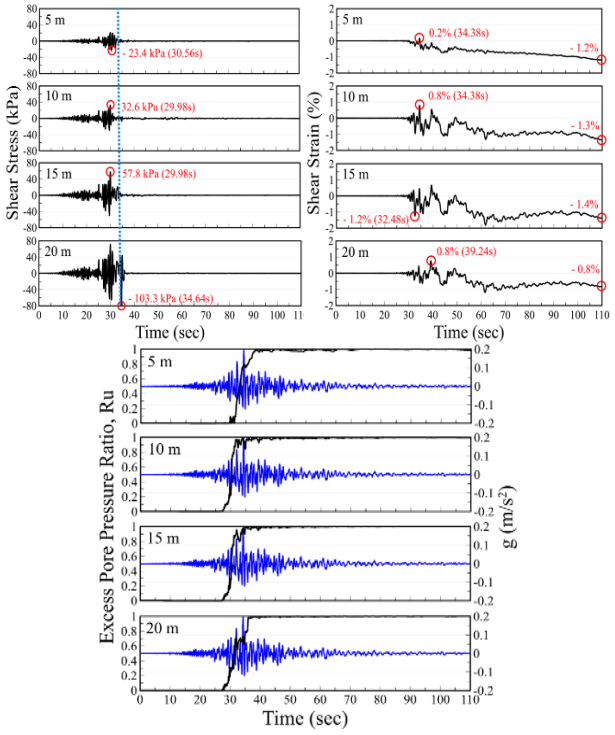

Figure 7. Results of 2D free-field model (PGA_T=0.195g).

5.2 *Raft and piled raft foundations*

With the standard single raft at the site, the modeling results are presented in Figure 8. The raft can decrease the permanent horizontal displacements for underneath soil; however, the total ground settlements were increased. As the seismic intensity has increased to 0.26g, more ground displacements can be found. Increasing the embedment depth seemed to cause large horizontal ground displacements. In addition, the raft was found uplifting if the raft is located below the groundwater table. Details can be found in Hsu (2025[b]).

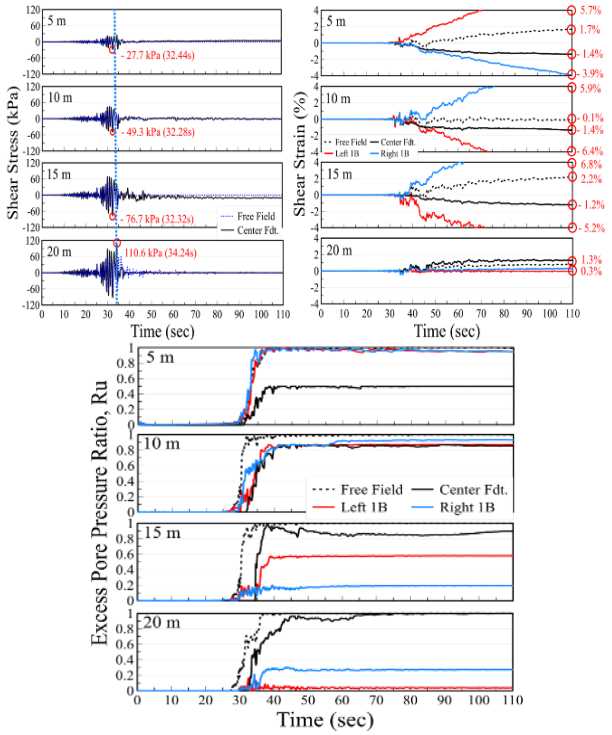

Figure 8. Results of 2D raft foundation model (PGA_T=0.195g).

For the piled raft foundation located at GL-2m at the site, the results are presented in Figure 9. It can be observed that the piled raft foundation can minimize the foundation settlements. However, the ratio of excess pore pressure became larger in this case. The foundation has no uplift occurred even it is below the groundwater table. The lateral ground displacements can be reduced compared to the single raft. Increasing the pile length and decreasing the pile-to-pile spacing distance for S/d=3~5 can help to gain the foundation resistance of low-rise building.

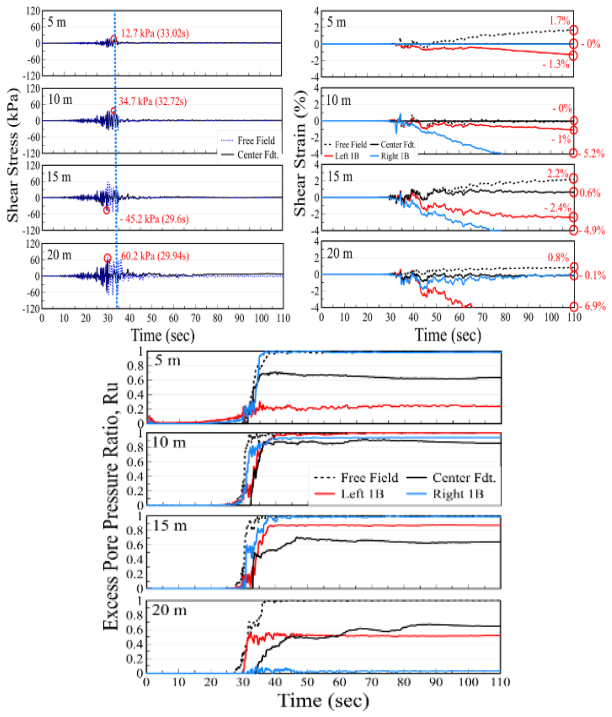

Figure 9. Results of 2D piled raft model (PGA_T=0.195g).

The corresponding plots of the total displacement field and the excess pore pressure ratio of the 2D analysis on the standard raft foundation at 0.26g are shown in Figures 10-11 at 90sec. The corresponding plots for the standard piled raft foundation at the end of the quake are presented in Figures 12-13. The soil liquefaction can affect the deeper soils at GL-20m~GL-30m if the raft foundation was installed. The ground soils moved equally to the lateral sides. For the piled raft foundation, the liquefaction was mostly occurring to the soils at the top 20m from the ground surface. The piled raft foundation can reduce the foundation settlement; however, the nearby ground surface could deteriorate like those found in the case of sole raft foundation.

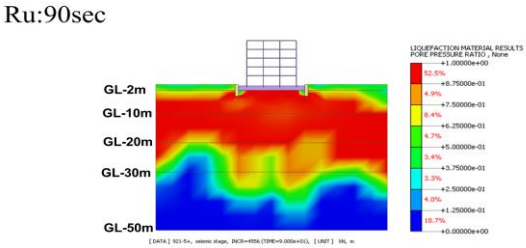

Figure 10. Excess pore pressure ratio (Ru) distributions of the sole raft foundation at 90 sec.

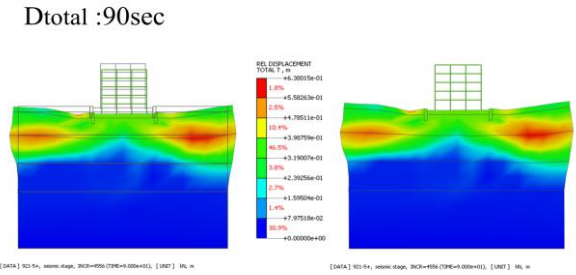

Figure 11. Total displacement field of the sole raft foundation at 90 sec.

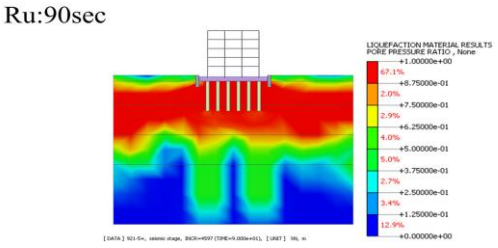

Figure 12. Excess pore pressure ratio (Ru) distributions of the piled raft foundation at 90 sec.

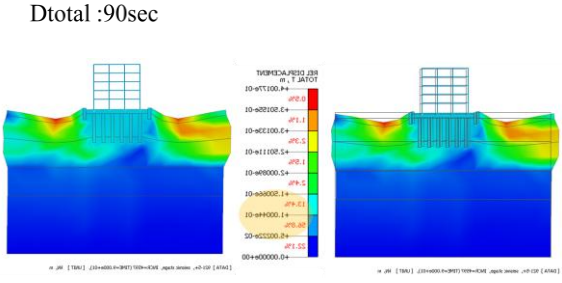

Figure 13. Total displacement field of the piled raft foundation at 90 sec.

For the comparisons of 2D and 3D analysis on piled raft foundation, the partial results from 3D analysis were presented in Figure14. It can be found that the Ru distribution was becoming more consistent, not that scattered found by the 2D analysis. The displacements caused in the 3D analysis are becoming smaller. At the present time, only a few cases of 3D analysis were conducted due to the computation time. The challenges arise to reach a feasible time of the required computations. Such issue is now considered with the soil-structure interactions of the building on the foundations.

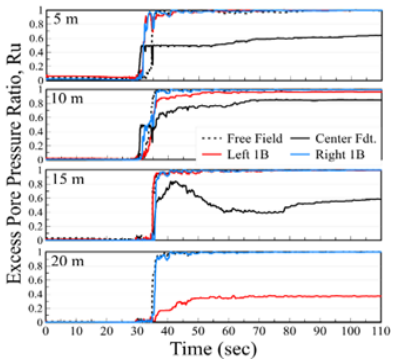

Figure 14. Results of excess porewater pressure ratio, Ru of 3D piled raft model (PGA_I=0.195g).

6 FREE-FIELD MEASURE COMPARISONS

Comparisons of the factors of safety against liquefaction for the free field site from the FE analysis (FEA) and the liquefaction potential analysis (LPA) methods were shown in Table 5. Note that the factor of safety from FE analysis was defined as the FS_1=1-Ru_{max} and FS_2=1/Ru_{max}, where Ru_{max} is the maximum value of the Ru. It was found that the different analysis results had comparable agreement. Nevertheless, the empirical methods are more conservative than the FE analysis on ground settlements (Hsu, 2025[a]).

Table 5. Comparisons of FS from LPA and FEA.

M	PGA	GL (m)	Factor of safety against soil liquefaction					
			Liquefaction potential analysis (LPA)				FE analysis	
			HBF	NCEER	AIJ	JRA	1-Ru_{max}	1/Ru_{max}
M=7.0 for LPA and M=7.3 for FEA	0.195g	-5	0.832	0.776	0.762	0.755	0	1
		-10	0.830	0.800	0.764	0.740	0	1
		-15	0.952	0.927	0.813	0.765	0	1
		-20	1.136	1.099	0.869	0.792	0	1
	0.26g	-5	0.623	0.583	0.572	0.566	0	1
		-10	0.622	0.600	0.573	0.555	0	1
		-15	0.713	0.696	0.610	0.574	0	1
		-20	0.852	0.824	0.652	0.594	0	1

7 FOUNDATION DAMAGE MEASURES

7.1 *Deformation modes*

The foundation deformations and their corresponding damage measures were illustrated and summarized in Figure 15 and Figure 16. Four deformation modes exerted on the raft slab of the foundation were analyzed. Only three of them were observed in this study.

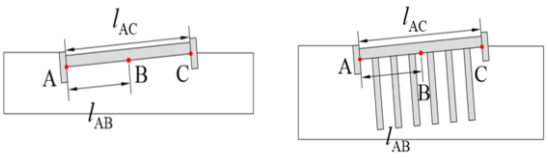

Figure 15. Layout of the distance between observation points.

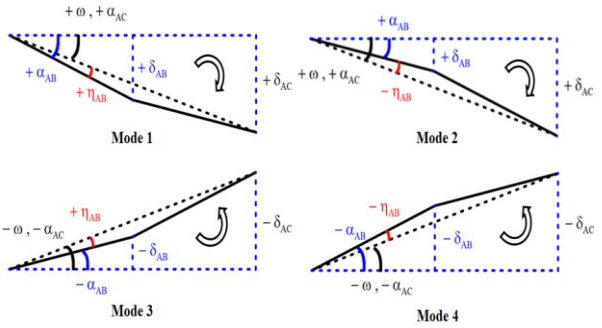

Figure 16. Damage models of the foundation.

Table 6. Damage measures of the foundations in this study.

Fdt.	Main variable(s)	Damage Measure							
		w_A (m)	δ_{AB} (m)	δ_{AC} (m)	α_{AB} (°)	α_{AC} (°)	ω	η_{AB}	mod
Raft	a_{max}=0.195g	0.4667	0.0163	0.0284	0.0934	0.0814	0.0014	0.0002	1
Raft	a_{max}=0.26g	0.9156	0.0154	0.0256	0.0882	0.0733	0.0013	0.0003	1
Raft	a_{max}=0.32g	1.0121	0.0188	0.0306	0.1077	0.0877	0.0015	0.0003	1
Raft	a_{max}=0.195g near-Fault	0.7363	0.0374	0.0703	0.2143	0.2014	0.0035	0.0002	1
Raft	a_{max}=0.26g near-Fault	1.0693	- 0.0381	- 0.0824	- 0.2183	- 0.2361	- 0.0041	0.0003	3
Raft	D_f=5m, a_{max}=0.195g	0.2854	0.0193	0.0343	0.1106	0.0983	0.0017	0.0002	1
Raft	D_f=5m, a_{max}=0.195g	- 0.0758	- 0.0384	- 0.0713	- 0.2200	- 0.2043	- 0.0036	- 0.0003	4
Raft	B=30m, a_{max}=0.195g	0.3155	0.0192	0.0264	0.0733	0.0504	0.0009	0.0004	1
Raft	q=50kPa, a_{max}=0.195g	1.2390	-0.0409	- 0.0995	- 0.2343	- 0.2850	- 0.0050	0.0009	3
PR.	a_{max}=0.195g	0.3391	0.0229	0.0229	0.1312	0.0656	0.0011	0.0011	1
PR.	a_{max}=0.26g	0.5631	-0.0378	-0.1042	-0.2166	-0.2985	-0.0052	0.0014	3
PR.	a_{max}=0.32g	0.5691	0.0439	0.0604	0.2515°	0.1730°	0.0030	0.0014	1
PR.	a_{max}=0.195g 3D analysis	0.2846	0.0422	0.0802	0.2418	0.2298	0.0040	0.0002	1
PR.	a_{max}=0.26g 3D analysis	0.5445	-0.0248	-0.0546	-0.1421°	-0.1564°	-0.0027	0.0003	3
PR.	D_f=5m, a_{max}=0.195g	0.1148	0.0132	0.0042	0.0756	0.0120	0.0002	0.0011	1
PR.	L=15m, a_{max}=0.195g	0.2382	-0.0251	-0.0606	-0.1495	-0.1736	-0.0030	0.0004	3
PR.	L=15m, a_{max}=0.195g 3D analysis	0.1163	0.0054	0.0093	0.0309°	0.0266°	0.0005	0.0001	1
PR.	S=5m, a_{max}=0.195g	0.4201	-0.0206	-0.0726	-0.1180	-0.2080	-0.0036	0.0016	3
PR.	B=30m, a_{max}=0.195g	0.2527	0.0216	-0.0180	0.1238	-0.0516	-0.0006	0.0020	3
PR.	q=50kPa, a_{max}=0.195g	0.6894	0.0564	0.0721	0.3231	0.2066	0.0036	0.0020	1

NOTE:
PR: piled raft, w_A: settlement at point A, "-" settlement means uplift, differential settlements δ_{AB}=W_B-W_A, δ_{AC}=W_C-W_A; tilt angle α "+" for clockwise rotation, "-" for counterclockwise rotation, α_{AB}=tan^{-1}(δ_{AB}/l_{AB}), α_{AC}=tan^{-1}(δ_{AC}/l_{AC}); rigid rotation angle ω=δ_{AC}/l_{AC}; angle variable η_{AB}=δ_{AB}/l_{AB} – ω. The sign of convention of ω is the same as α. For "+" angle variable, raft bent upward, for "-" angle variable, raft bent downward.

7.2 *Settlements, tilts and angle variables*

Table 6 summarizes the foundation displacements and the corresponding tilt angles. The differential settlements (δ) were able to compute from the left corner (point A) to the center (point B) and to the right corner (point C). Dividing the differential settlements (δ) with the horizontal distance (l) between arbitrary locations can result in the tilt angles (α). Subtracting the rigid rotation angle (ω) from the tilt angle can yield an angle variable (η). According to the design code, the angle variable (η) at 1/500 can cause the building to crack. In general, the studies indicated that the numerical foundations could behave rigidly by implementing a 1.5m-thick raft. Since

the maximum foundation settlement needs to be controlled under 30cm, the piled raft with the minimum pile length of 15m was recommended rather than the single raft.

8 CONCLUSIONS

The applicability of the raft and the piled raft foundation for the low-rise building on liquefiable soil profile was investigated numerically in this study. At the seismic intensity levels V^+ (PGA_T=0.195g) and VI^- (PGA_T=0.26g), large foundation settlements (>30cm) were observed for raft foundations. The 1.5m thick slab can yield a rigid foundation rotation in which the angle variable is restraint according to the design code. However, the corresponding rotation angle can still cause minor damage to the building. If the raft was located below the groundwater table and soil liquefaction occurred, the raft could cause uplift problems. In contrast, the use of piled raft foundation can yield less settlements. In such case, longer piles with 15m pile length were recommended. Lowering the groundwater table seems to be an alternate solution. The 2D analysis seemed to provide conservative estimates rather than the 3D analysis. However, since only a few 3D analyses were conducted, it needs more investigations for clarification. In general, if soil liquefaction occurred, the vertical ground displacements were found to be larger than horizontal ground displacements. If the near-fault effect was considered, the foundation settlements can be enlarged significantly. In such cases, the piled raft foundation is suggested. The results from liquefaction potential analysis indicate that the empirical estimations of soil liquefaction are agreeable to the FE analysis. However, the seismic settlements predictions from these methods are more conservative than the FE analysis.

9 ACKNOWLEDGEMENTS

This paper presents a partial result from the research grants NSTC-112-2625-M-032-005 and NSTC-113-2625-M-032-001 of the National Science and Technology Council in Taiwan. Financial support is greatly appreciated by the authors.

10 REFERENCES

Byrne, P.M., Park, S.S., and Beaty, M. 2003. Seismic liquefaction: centrifuge and numerical modeling, in International FLAC Symposium; FLAC and numerical modeling in geomechanics, 321-332.

Byrne, P.M., Park, S.S., Beaty, M., Sharp, M.K., Gonzalez, L. and Abdoun, T. 2004. Numerical modeling of liquefaction and comparison with centrifuge tests, *Canadian Geotechnical Journal*, 41(2), 193-211.

Hsu, C.Y. 2025[a]. *Study on liquefaction potential assessment and empirical methods for seismic settlements*, Master Thesis, Dept. of Civil Engr, Tamkang University, Taiwan (in Chinese).

Hsu, T.L. 2025[b]. *Seismic performance of direct foundation and pile-raft foundation for low-rise structure in liquefaction sites*, Master Thesis, Dept. of Civil Engr, Tamkang University, Taiwan (in Chinese).

Idriss, I.M. and Boulanger, R.W. 2008. *Soil liquefaction during earthquakes. Monograph MNO-12*, Earthquake Engineering Research Institute, Oakland, CA, 2008, 261 pp.

Ishihara, K. and Yoshimine, M. 1992. Evaluation of settlements in sand deposits following liquefaction during earthquake, *Soils and Foundations*, 32(1), 173-188.

Ko, Y.Y. 2023. CTX and CSST Data, Personal communications.

Kramer, S.L. and Stewart, J.P. 2024. *Geotechnical Earthquake Engineering*, CRC Press, 1060 pp.

Lien, X.J. 2024. *Effects of light-weight structure direct foundation on earthquake induced soil liquefaction*, Master Thesis, Dept. of Civil Engr, Tamkang University, Taiwan. (in Chinese)

Lu, C.C., Hwang, J.H., and Hsu, S.Y., 2017. The impact evaluation of soil liquefaction on low-rise building in the Meinong earthquake, *Earth, Planets and Space*, 69(109), 1-16

Midas 2020. Midas-GTS NX, User Manual.

Ministry of Interior 2023. *The Building Foundation Structure Design Code*, Taiwan.

Tokimatsu, K. and Seed, H.B. 1987. Evaluation of settlements in sands due to earthquake shaking. *Journal of Geotechnical Engineering,* ASCE, 113(8), 861-878.